Improving high-temperature performance in continuous-wave mode InGaAsN/GaAsN ridge waveguide lasers

2005 Semicond. Sci. Technol. 20 601

(http://iopscience.iop.org/0268-1242/20/6/020)

INSTITUTE OF PHYSICS PUBLISHING SEMICONDUCTOR SCIENCE AND TECHNOLOGY
Semicond. Sci. Technol. **20** (2005) 601–605 doi:10.1088/0268-1242/20/6/020

Improving high-temperature performance in continuous-wave mode InGaAsN/GaAsN ridge waveguide lasers

Yi-An Chang[1], Hao-Chung Kuo[1], Chun-Yi Lu[1], Yen-Kuang Kuo[2] and Shing-Chung Wang[1]

[1] Institute of Electro-Optical Engineering, National Chiao-Tung University, Hsinchu 300, Taiwan
[2] Department of Physics, National Changhua University of Education, Changhua 500, Taiwan

E-mail: hckuo@faculty.nctu.edu.tw

Received 28 December 2004, in final form 31 March 2005
Published 27 April 2005
Online at stacks.iop.org/SST/20/601

Abstract
Continuous-wave (CW) mode operation InGaAsN/GaAsN double-quantum-well lasers with a laser wavelength of 1.295 μm are demonstrated by metal-organic chemical vapour deposition (MOCVD). With the use of a high-bandgap $GaAs_{0.9}P_{0.1}$ into the active region before the growth of p-type layers, a room temperature (RT) threshold current of 99 mA and the characteristic temperature (T_0) values of 155 K in a temperature range of 25–95 °C and 179 K in a temperature range of 25–85 °C are obtained from a 4 × 1000 μm^2 ridge waveguide uncoated laser diode. The T_0 value of the conventional structure without the high-bandgap $GaAs_{0.9}P_{0.1}$ is 118 K in a temperature range of 25–95 °C. High-temperature performance is improved and the results of numerical analysis suggest that it may be attributed to the reduced electronic leakage current.

1. Introduction

The startling progress of InGaAs with dilute nitride material has unmitigatedly continued to the present since the first proposition of Kondow *et al* in 1997 [1]. This novel material has demonstrated higher crystal quality [2, 3] than anticipated, possessing better high-temperature operation performance due to the increased band offsets and a more favourable band-offset ratio [4, 5]. Unfortunately, these devices show only a slight improvement in the T_0 values of 70–110 K over those achievable by the conventional InP technology under CW mode operation [6–10]. The unexpected low T_0 value is found due to the large Auger recombination and nitrogen penalty [11, 12]. To improve the lasing characteristics and high-temperature operation performance, using anti-reflection–high-reflection facet coating can obtain a CW output power of 210 mW [13], and Qu *et al* fabricated laser chips that were bonded p-side-down onto a copper heat-sink with pulsed anodic oxidation (PAO) technology, which could operate in CW mode up to 130 °C with a high T_0 value of 138 K [14]. In the case of laser structure design for improving lasing characteristics or obtaining a better T_0 value, Tansu *et al* utilized tensile-strain $GaAs_{0.85}P_{0.15}$ layers on both sides of the InGaAsN/GaA's active region to reduce the strain in quantum wells (QWs) for achieving better crystal quality [15–17].

However, the high-bandgap $GaAs_{0.85}P_{0.15}$ layer on the n-side InGaAsN/GaAs active region may obstruct electrons pouring into the active region, while the $GaAs_{0.85}P_{0.15}$ layer on the p-side active region can block electrons overflowing to the p-side layers. In a previous work, we had numerically investigated the laser performances and the T_0 values of $In_{0.4}Ga_{0.6}As_{0.986}N_{0.014}/GaAs_{1-x}N_x$ quantum-well lasers with variant $GaAs_{1-x}N_x$ strain-compensated barriers. The results from numerical analysis acquainted that using $GaAs_{1-x}N_x$ strain-compensated barriers with an x value less than 0.5% might provide better optical gain properties and a higher T_0 value. The electronic leakage current also played an important role in the decreased T_0 value [18]. To achieve a more favourable T_0 value, the $In_{0.41}Ga_{0.59}As_{0.987}N_{0.013}/GaAs_{0.995}N_{0.005}$ QW laser structure with a high-bandgap 15 nm thick $GaAs_{0.9}P_{0.1}$ layer inserted into the active region before the growth of p-type layers of

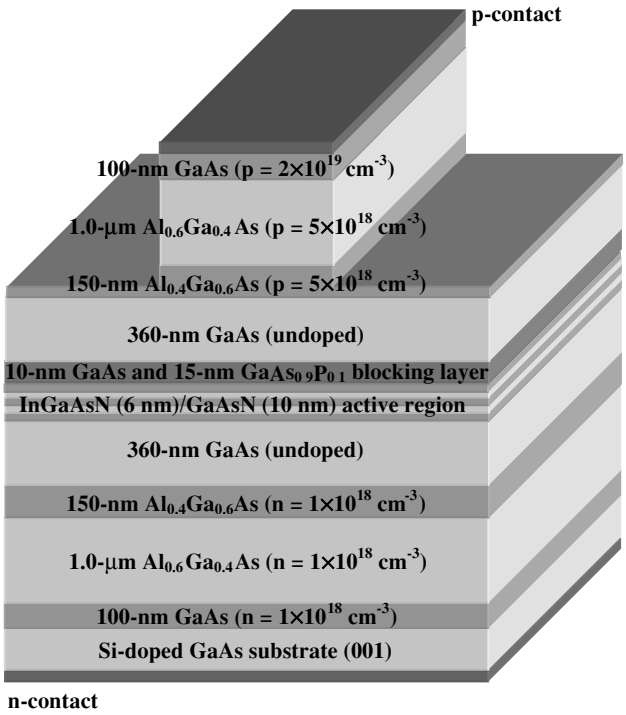

Figure 1. A schematic diagram of the DQW InGaAsN/GaAsN laser structure.

the conventional structure is conducted experimentally and numerically in this work.

2. Device structure and methods

The laser structure under study is grown by low pressure metal-organic chemical vapour deposition (MOCVD) with group-V precursors of arsine (AsH_3), phosphine (PH_3) and U-dimethylhydrazine (U-DMHy) for N-precursor. Trimethyl (TM) sources of aluminium (Al), gallium (Ga) and indium (In) are used for group-III precursors. The dopant sources are SiH_4 and CBr_4. The device is prepared by photolithography and reactive ion-etching into narrow stripe ridge waveguide lasers 4 μm in width and 1000 μm in length. The end facets of the laser chips are uncoated and the laser chips are bonded p-side-down onto copper heat-sinks with indium. A schematic diagram of the double-quantum-well (DQW) InGaAsN/GaAsN laser structure is plotted in figure 1. The InGaAsN/GaAsN ridge waveguide DQW laser structure is grown on the n-type Si–GaAs substrate with (0 0 1) orientation.

On top of the GaAs template is a 1.0 μm thick n-type $Al_{0.6}Ga_{0.4}As$ layer, followed by a 0.15 μm thick n-type $Al_{0.4}Ga_{0.6}As$ layer with a growth temperature of 770 °C. The active region contains two $In_{0.41}Ga_{0.59}As_{0.987}N_{0.013}$ wells and the growth temperature is 530 °C with a V/III ratio of 20. To reduce the high strain in the $In_{0.41}Ga_{0.59}As_{0.987}N_{0.013}$ QW, $GaAs_{0.995}N_{0.005}$ is used as a barrier. The thickness of QW and barrier is determined by x-ray diffraction. The strains of QW and barrier are 2.08% in compressive and 0.2% in tensile, respectively. After the growth of the active region, a 10 nm thick undoped GaAs layer is grown to cap the active region for maintaining better QW quality and a 15 nm thick undoped high-bandgap $GaAs_{0.9}P_{0.1}$ layer is grown to block electrons from overflowing to the p-type layers. The guiding region is formed by 0.72 μm thick undoped GaAs with a growth temperature of 530 °C, followed by a 0.4 μm thick p-type $Al_{0.4}Ga_{0.6}As$ layer with a doping concentration of 5×10^{18} cm^{-3} and a 1.0 μm thick p-type $Al_{0.6}Ga_{0.4}As$ layer with a doping concentration of 5×10^{18} cm^{-3}. Finally, a p-type 100 nm thick GaAs layer with a doping concentration of 2×10^{19} cm^{-3} is grown to complete the structure.

Numerical simulation is executed with the use of an advanced two-dimensional LASer Technology Integrated Program (LASTIP), which is a full two-dimensional (2D) simulator that solves Poisson's equation, current continuity equations, the photon rate equation and the scalar wave equation. In the gain model, material gain and loss for both bulk and QW as functions of wavelength and carrier density are computed. Two-dimensional drift–diffusion semiconductor equations are solved for the drift–diffusion model, which is similar to a conventional 2D electronic device simulator except that stimulated and spontaneous emissions of a laser are included as additional recombination terms. In the optical mode model, a 2D scalar complex wave equation is solved for the lateral modes. The photon rate equation, which couples to the drift–diffusion equations, is also solved. Complex refractive indices computed from the material gain are required as inputs [19].

For the numerical simulation, based on $k \cdot p$ theory, a Hamiltonian matrix of the Luttinger–Kohn type and an envelope function approximation are used to solve the InGaAsN quantum-well subband structures and the gain spectra are broadened by Lorentz's function. The band-offset ratios of InGaAsN and GaAsP to GaAs are estimated to be 0.7/0.3 and 0.58/0.42, respectively [4, 20]. The room temperature (RT) bandgap energies of GaAs, InAs, GaN and InN are 1.424, 0.355, 3.42 and 0.77 eV, respectively [21]. The temperature dependence of the bandgap energies is governed by the Varshini equation and the RT bandgap energy of $In_{0.41}Ga_{0.59}As_{0.987}N_{0.013}$ is about 0.73 eV. The effective masses of electrons in GaAs, InAs, GaN and InN alloys are $0.064 \times m_0$, $0.023 \times m_0$, $0.2 \times m_0$ and $0.11 \times m_0$ respectively, while the effective masses of light holes (LH) and heavy holes (HH) are $0.091 \times m_0$ and $0.37 \times m_0$ for GaAs, $0.027 \times m_0$ and $0.814 \times m_0$ for InAs, $0.977 \times m_0$ and $1.376 \times m_0$ for GaN and $0.513 \times m_0$ and $1.595 \times m_0$ for InN, respectively. The effective mass of electrons in $In_{0.41}Ga_{0.59}As_{0.987}N_{0.013}$ is $0.053 \times m_0$, and the effective masses of LH and HH in $In_{0.41}Ga_{0.59}As_{0.987}N_{0.013}$ are $0.079 \times m_0$ and $0.354 \times m_0$, respectively. A large background loss value of 25 cm^{-1} is used and other material-dependent parameters are taken from [22] and the default database values given in the material macro file [19].

3. Laser characteristics

For the discussion of the effect of the $GaAs_{0.9}P_{0.1}$ current blocking layer on the laser performance of the $In_{0.41}Ga_{0.59}As_{0.987}N_{0.013}/GaAs_{0.995}N_{0.005}$ laser, two structures that are without and with inserting the high-bandgap $GaAs_{0.9}P_{0.1}$ into the active region before the growth of p-type layers are prepared. The DQW structure for type A is the conventional structure without the high-bandgap $GaAs_{0.9}P_{0.1}$

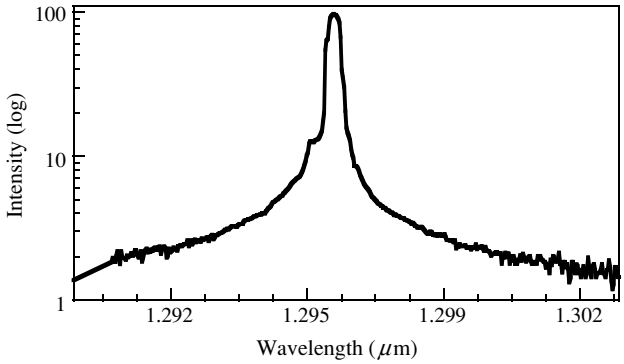

Figure 2. Electroluminescence spectrum when the laser device is at an input current of laser threshold.

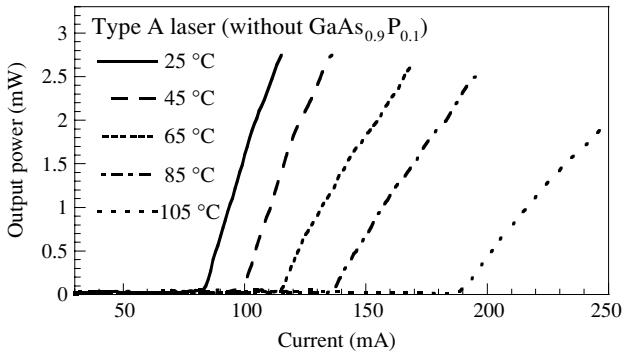

Figure 3. Temperature-dependent *L–I* characteristic of the type A laser under CW mode operation in a temperature range of 25–105 °C.

inserted and type B is the structure with the high-bandgap $GaAs_{0.9}P_{0.1}$ inserted. The laser devices are tested under CW mode operation. Figure 2 shows the electroluminescence spectrum when the laser device is at an input current of laser threshold. A peak emission wavelength of 1.295 μm is obtained for both type A and type B lasers.

The temperature-dependent laser output power versus current (*L–I*) characteristic of the type A laser under CW mode operation in a temperature range of 25–105 °C is shown in figure 3. The stripe width and the cavity length are 4 μm and 1000 μm, respectively. The threshold current and the threshold current density per QW are 84 mA and 1.05 kA cm^{-2} at 25 °C. Figure 4 shows the temperature-dependent *L–I* characteristic of the type B laser under CW mode operation in a temperature range of 25–105 °C. The stripe width and the cavity length are identical to the type A laser. The threshold current is 99 mA and the threshold current density per QW is 1.23 kA cm^{-2} at 25 °C. The RT slope efficiencies of type A and type B lasers are 0.09 and 0.11 W A^{-1}.

Despite the high threshold current density at 25 °C, which is caused by the high strain in the quantum wells and the non-radiative recombination centres, it is found that the slope efficiency is increased after inserting the high-bandgap $GaAs_{0.9}P_{0.1}$. For the type A laser, the threshold current increases from 84 to 152 mA, and a T_0 value of 118 K under CW mode operation is achieved when the device temperature is in the range of 25–95 °C. With the use of $GaAs_{0.9}P_{0.1}$ in the p-side active region, the T_0 value under CW mode operation is ameliorated to 155 K in a temperature range of 25–95 °C. The

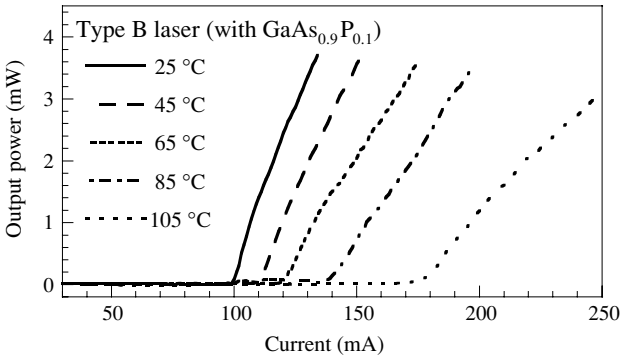

Figure 4. Temperature-dependent *L–I* characteristic of the type B laser under CW mode operation in a temperature range of 25–105 °C.

T_0 value can achieve up to 179 K when the device temperature is in a range of 25–85 °C. As the device temperature is higher than 105 °C, the threshold current of the type B laser is lower than that of the type A laser, which indicates that the electronic leakage current is reduced and the hole injection into the active region is improved at a higher temperature when the high-bandgap $GaAs_{0.9}P_{0.1}$ is inserted into the active region before the growth of p-type layers. The threshold currents of type A and type B are 188 mA and 173 mA, respectively, when the device temperature is 105 °C. The high T_0 value obtained may be partially due to the decreased electronic leakage current and the slightly increased threshold current at 25 °C and monomolecular defect recombination [23].

4. Numerical analysis

Based on the experimental results that the high-temperature performance is improved by inserting a high-bandgap $GaAs_{0.9}P_{0.1}$ layer into the active region before the growth of p-type layers, we further theoretically investigate the effect of the high-bandgap $GaAs_{0.9}P_{0.1}$ layer on the laser performance of the 4 $\times$ 1000 μm^2 $In_{0.41}Ga_{0.59}As_{0.987}N_{0.013}/GaAs_{0.995}N_{0.005}$ DQW laser. The threshold currents and slope efficiencies of type A and type B lasers obtained experimentally and numerically are depicted in figure 5. It is found that the simulation results fit in with the experiments. Results of numerical simulation also indicate that the use of $GaAs_{0.9}P_{0.1}$ can beneficially improve the high-temperature performance, and an increased T_0 value from 107 to 130 K in a temperature range of 25–95 °C is anticipated, even though the T_0 value is not very consistent with the experiments. The discrepancy in the slope efficiencies obtained from the simulations compared to the experiments is due to the fact that we assume the laser device to be isothermal in simulation and the thermal effects are arduous to be completely considered.

The RT energy band diagrams of type A and type B lasers are shown in figure 6. The diagrams are obtained when the input current is 250 mA and the applied voltage is 1.63 V. The left-hand side of the diagrams is the n-side of the laser structure and the dashed lines are quasi-Fermi levels. It is shown that the high-bandgap $GaAs_{0.9}P_{0.1}$ is in the p-side of the active region and acts as an electronic blocking layer to prevent the electronic current overflow. However,

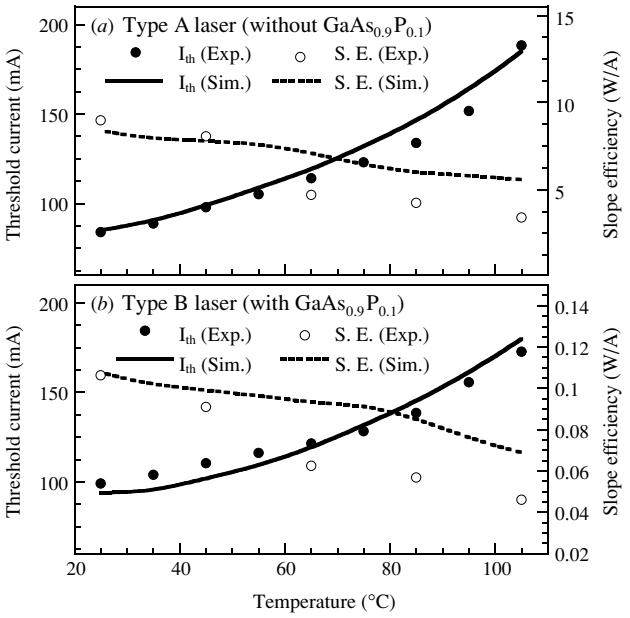

Figure 5. Threshold currents and slope efficiencies of type A and type B lasers obtained experimentally and numerically.

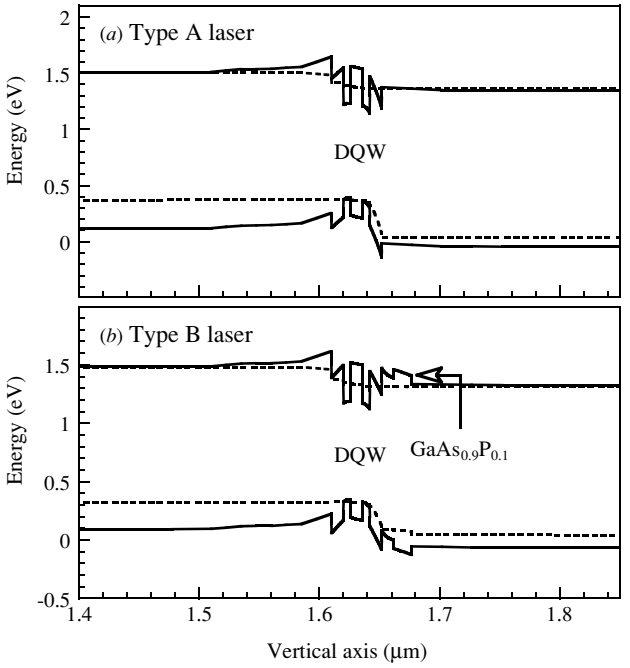

Figure 6. RT energy band diagrams of type A and type B lasers.

a barrier height in the valence band of inserting the high-bandgap $GaAs_{0.9}P_{0.1}$, shown in figure 6(*b*), is found and this may result in the difficulty of hole injection and the increased threshold current. The increased threshold current caused by inserting $GaAs_{0.9}P_{0.1}$ may also be attributed to the slight decrease of optical confinement factor from 7.4% to 7.2% and the blemished interface between $GaAs_{0.9}P_{0.1}$ and GaAs in crystal growth.

Figure 7 illustrates the percentage of electronic leakage current obtained numerically as a function of device temperature for type A and type B lasers. The results are obtained when the devices are at an input current of 250 mA

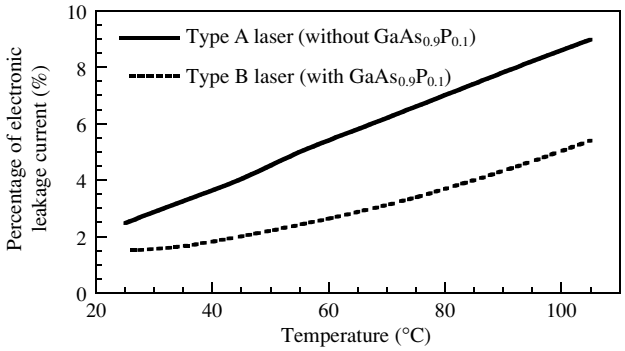

Figure 7. Percentage of electronic leakage current obtained numerically as a function of device temperature for type A and type B lasers.

and the percentage of the electronic leakage current is defined as the ratio of the current overflow to the p-type layer to that injected into the active region. Note that the percentage of electronic leakage current increases with device temperature for both the laser structures. With the help of the increased conduction band offset caused by inserting $GaAs_{0.9}P_{0.1}$, the percentage of electronic leakage current is apparently reduced, in turn decreasing the threshold current at a higher temperature. When the device temperature is 95 °C, there are 8.2% and 4.7% current overflows for type A and type B lasers, respectively, and the percentage of electronic leakage current increases more rapidly for the laser structure without the $GaAs_{0.9}P_{0.1}$.

5. Conclusion

This study demonstrates the T_0 values of 155 K in a temperature range of 25–95 °C and 179 K in a temperature range of 25–85 °C for a CW mode operation narrow stripe $4 \times 1000\,\mu m^2$ $In_{0.41}Ga_{0.59}As_{0.987}N_{0.013}/GaAs_{0.995}N_{0.005}$ laser diode with the use of a high-bandgap 15 nm thick $GaAs_{0.9}P_{0.1}$ electronic blocking layer. The temperature-dependent *L–I* characteristics obtained from simulations are in close agreement with those obtained from experiments. With an advanced two-dimensional LASTIP simulation program, the improved laser performances at high temperature are found to be due to the decreased electronic leakage current. When the device is at an input current of 250 mA, with the use of the $GaAs_{0.9}P_{0.1}$, the percentage of electronic leakage current is reduced from 8.2% to 4.7% at a device temperature of 95 °C. The results obtained experimentally and numerically also indicate that the electronic leakage current begins to affect the laser performance when the device temperature is higher than 95 °C.

Acknowledgments

The authors would like to give their sincere appreciation to the Crosslight Incorporation for providing the advanced two-dimensional LASTIP simulation program (version 2003.12) and Professor Nelson Tansu in Leigh University, USA, for the precious discussion. This work is supported by the National Science Council, Republic of China, under grant NSC-93-2120-M009-006 and by the Academic Excellence Program of the Ministry of Education of ROC under the contract NSC-93-2752-E009-008.

References

[1] Kondow M, Kitatani T, Nakatsuka S, Larson M C, Nakahara K, Yazawa Y, Okai M and Uomi M 1997 *IEEE J. Sel. Top. Quantum Electron.* **3** 719

[2] Buyanova I A, Izadifard M, Chen W M, Polimeni A, Capizza M, Xin H P and Tu C W 2003 *Appl. Phys. Lett.* **82** 3662

[3] Albrecht M, Grillo V, Remmele T, Strunk H P, Egorov A Yu, Dumitras Gh, Riechert H, Kaschner A, Heitz R and Hoffmann A 2002 *Appl. Phys. Lett.* **81** 2719

[4] Bellaiche L, Wei S-H and Zunger A 1996 *Phys. Rev.* B **54** 17568

[5] Heroux J B, Yang X and Wang W I 2003 *IEE Proc. Optoelectron.* **150** 92

[6] Gollub D, Moses S, Fischer M and Forchel A 2003 *Electron. Lett.* **39** 777

[7] Tansu N, Kirsch N J and Mawst L J 2002 *Appl. Phys. Lett.* **81** 2523

[8] Peng C S, Jouhti T, Laukkanen P, Pavelescu E-M, Konttinen J, Li W and Pessa M 2002 *IEEE Photon. Technol. Lett.* **14** 275

[9] Livshits D A, Egorov A Y and Riechert H 2000 *Electron. Lett.* **36** 1381

[10] Wei J, Xia F, Li C and Forrest S R 2002 *IEEE Photon. Technol. Lett.* **14** 597

[11] Polyakov A Y *et al* 2002 *Solid-State Electron.* **46** 2147

[12] Fehse R, Tomic S, Adams A R, Sweeney S J, O'Reilly E P, Andreev A and Riechert H 2002 *IEEE J. Sel. Top. Quantum Electron.* **8** 801

[13] Kovsh A R, Wang J S, Hsiao R S, Chen L P, Livshits D A, Lin G, Ustinov V M and Chi J Y 2003 *Electron. Lett.* **39** 1726

[14] Qu Y, Liu C Y, Ma S G, Yuan S, Bo B, Liu G and Jiang H 2004 *IEEE Photon. Technol. Lett.* **16** 2406

[15] Tansu N, Yeh J Y and Mawst L J 2003 *Appl. Phys. Lett.* **82** 3008

[16] Tansu N, Quandt A, Kanskar M, Mulhearn W and Mawst L J 2003 *Appl. Phys. Lett.* **83** 18

[17] Tansu N and Mawst L J 2002 *IEEE Photon. Technol. Lett.* **14** 444

[18] Chang Y-A, Kuo H-C, Chang Y-H and Wang S-C 2004 *Opt. Commun.* **241** 195

[19] *LASTIP User's Manual Version 2003.12* 2003 Crosslight Inc. Software, Canada http://www.crosslight.ca

[20] Hou H Q, Tu C W, Shan W, Hwang S J, Song J J and Chu S N G 1993 *J. Vac. Sci. Technol.* B **11** 854

[21] Wu J, Walukiewicz W, Yu K M, Ager J W III, Haller E E, Lu H and Schaff W J 2002 *Appl. Phys. Lett.* **80** 4741

[22] Vurgaftman I and Meyer J R 2003 *J. Appl. Phys.* **94** 3675

[23] Tansu N, Chang Y-L, Takeuchi T, Bour D P, Corzine S W, Tan M R T and Mawst L J 2002 *IEEE J. Quantum Electron.* **38** 640